ISSN 1068-3755, Surface Engineering and Applied Electrochemistry, 2007, Vol. 43, No. 6, pp. 443–452. © Allerton Press, Inc., 2007.
Original Russian Text © O.L. Bersirova, L.I. Bruk, A.I. Dikusar, M.I. Karaman, S.P. Sidel'nikova, A.V. Simashkevich, D.A. Sherban, Yu.S. Yapontseva, 2007, published in Elektronnaya Obrabotka Materialov, 2007, No. 6, pp. 40–49.

Thin Films of Titanium and Tin Oxides and Semiconductor Structures on Their Basis Obtained by Pyrolytic Pulverization: Preparation, Characterization, and Corrosion Properties

O. L. Bersirova[b], L. I. Bruk[c], A. I. Dikusar[a], M. I. Karaman[c], S. P. Sidel'nikova[a], A. V. Simashkevich[a], D. A. Sherban[a], and Yu. S. Yapontseva[b]

[a] *Institute of Applied Physics, Academy of Sciences of Moldova, ul. Akademiei 5, Chisinau, MD-2028 Moldova*
[b] *Vernadskii Institute of General and Inorganic Chemistry, National Academy of Sciences of Ukraine, pr. Akademika Palladina 32/34, Kiev-142, 03680 Ukraine*
[c] *Moldova State University, ul. Mateevicha 60, Chisinau, MD-2012 Moldova*

Received August 2, 2007

Abstract—Peculiarities of obtaining of tin oxide and titanium oxide layers and semiconductor structures on their basis are described. The X-ray diffraction data show that the SnO_2 and TiO_2 layers possess the tetragonal crystal structure (anatase modification for TiO_2). The results of analysis of the elemental composition and impedance investigations of the fabricated structures in model chloride–sulfate solutions demonstrate that the oxide/SiO_2/Si structures are obtained if Si substrates are used. In the case of InP substrates, the oxide layer at the interface is not detected and the corresponding structure is oxide/InP. The results of investigations of corrosion show that a substantial shift of the corrosion potential to the anode region is observed in the case of deposition of SnO_2 and TiO_2 oxide layers on Si and InP crystals and fabrication of corresponding semiconductor structures. This demonstrates the possibility of the use of these materials in photoelectrochemical applications.

DOI: 10.3103/S1068375507060075

INTRODUCTION

It is known that, on the base of transparent conducting metal oxides (TCO) such as SnO_2, In_2O_3, TiO_2, and ITO, semiconductor–insulator–semiconductor (SIS) structures are formed, which are used for conversion of solar energy into electric energy [1–5]. In such structures, silicon and semiconductor III–V compounds, for example, indium phosphide, are mainly used as materials absorbing solar radiation. The TCO layers are the components of not only of photovoltaic but also of photoelectrochemical cells [6, 7], where they play the protective role against corrosion of the matrix semiconductor material. Wide-gap oxide layers, in addition to the immediate anticorrosion function, also promote the extension of the spectral characteristics of the photosensitivity due to a decrease in the surface recombination in the narrow-gap absorbing material. In addition, the SnO_2 and TiO_2 layers can be successfully used in Si-based and InP-based solar cells as an antireflection coating due to their transparency in the visible spectral range and appropriate values of the refraction indices (n = 2.0 and n = 1.72–2.60, respectively), which increases the efficiency of transformation of solar energy into electric energy.

Properties of semiconductor films and structures are largely determined by the technology of their preparation. However, there are few works in the available literature where the properties of these materials, specifically photocorrosion properties, are described depending on the conditions of their obtaining. In this work, we describe the technology of obtaining the SnO_2-based and TiO_2-based layers and heterostructures as well as investigation of their structural, optical, and photocorrosion properties. The used method of pyrolytic pulverization for obtaining the layers and structures is rather simple and economical, does not require complex equipment, and can be used for obtaining efficient photovoltaic converters.

EXPERIMENTAL

The TiO_2 and SiO_2 films were formed during deposition of $TiCl_4$ solutions in ethyl acetate, ethanol, or $SnCl_4$ in ethanol on the substrates heated to 450°C. The substrates were quartz, sapphire, as well as Si and InP. Depending on the concentration of the used solutions and sprayed volumes, their nature, and the substrate, the films were of various thicknesses (from 50 to 400 nm).

To obtain SnO_2, we used a 0.5 M $SnCl_4$ solution in ethanol. In certain cases, for doping of the film by antimony, a 0.1 M $SbCl_3$ solution in ethanol was used. To prepare the solution with a dopant, up to 2 ml of the 0.1 M $SbCl_3$ solution was added to 11 ml of the 0.5 M $SnCl_4$ solution. To obtain the TiO_2 layers, we used solu-

tions prepared by mixing of a 1 M $TiCl_4$ solution and the solvent in the following ratios: 1 : 1, 1 : 2, and 1 : 3.

During pulverization in air and subsequent pyrolysis, a series of reactions proceeds. These reactions, which are associated with hydrolysis, evaporation, and oxidation, in the general form, can be presented as follows:

$$TiCl_4 + O_2 = TiO_2 + 2Cl_2,$$

$$SnCl_4 + O_2 = SnO_2 + 2Cl_2, \quad (1)$$

$$4SbCl_3 + 3O_2 = 2Sb_2O_3 + 6Cl_2.$$

To obtain the films, equipment preliminary described in [15] was used.

The structure was analyzed by X-ray diffraction with the use of a Brucker linear diffractometer (CuK_α radiation, Ni filter, θ–2θ scanning).

In this work, we used the following methods of analysis of the composition and morphology of the obtained films:

(i) scanning electron microscopy (SEM) with the use of a TESCAN VEGA scanning electron microscope;

(ii) a system for investigation of the chemical composition (INGA Energy EDX) for determination of the elemental composition. A special feature of the method used in this investigation consisted of performing the analysis over a region with a diameter of several micrometers to a depth of up to 2 μm. The analysis was carried out at three points of each sample, after which the average value was calculated. The interval values given below correspond to standard deviations from the average value.

The transmission and reflection spectra of the SnO_2 and TiO_2 layers obtained on various substrates (glass, quartz, sapphire) were measured using a Specord spectrophotometer in the wavelength range of 0.2–1.5 μm.

The photocorrosion of the obtained layers and narrow-gap semiconductors on which they were deposited (Si, InP) was investigated by two methods, namely, electrochemical impedance spectroscopy and voltammetry using an AUTOLAB (GPSTAT 20+FRA) system with GPES 4.9 and FRA 4.9 software. The current–voltage measurements were carried out both in the dark and in the light. In the first case, the electrochemical cell was coated with a material not transmitting the light, and, in the second case, the measurements were carried out under illumination by an incandescence lamp with a power of 60 W, which was arranged at a distance of approximately 30 cm from the measuring cell. The corrosion behavior of all the samples was investigated in a neutral (pH = 6.0 ± 0.1) medium. As a model solution, we selected a solution of a mixture of sulfates and chlorides (7 g/l Na_2SO_4 + 7 g/l NaCl). The measurements were carried out at a temperature of 24 ± 1°C in the cell with a saturated silver–silver chloride electrode and an auxiliary electrode in the form of a platinum grid. All the values of the potentials are given relative to the saturated silver–silver chloride electrode.

The spectra of the electrochemical impedance were recorded after holding the sample in the corrosion solution for 15 min to establish the steady-state potential. The voltage was supplied sinusoidally with an amplitude of 5 mV. The spectra are obtained in a frequency range of 50 kHz–1 MHz. The parameters of the corrosion process and corresponding equivalent circuits were determined based on the analysis of these spectra.

The current–voltage measurements consisted of obtaining the anode and cathode polarization curves for a rate with specifying a potential of 1 mV/s. The polarization curves were corrected by the magnitude of the ohmic voltage drop IR. Based on the obtained curves, the corrosion characteristics were calculated.

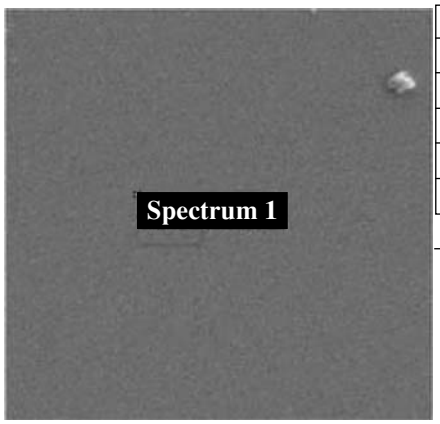
RESULTS AND DISCUSSION

Chemical Composition of the Films and Heterostructures Obtained on Various Substrates and Peculiarities of the Interrelation of the Measured Chemical Composition and Film Thickness

The chemical composition of the films during their deposition on transparent materials (glass, sapphire) and heterostructures obtained on their deposition on Si and InP, as was already noted above, was carried out using a variant of EDX analysis in which the surface layer with a thickness of 2–3 μm was studied. It is evident that, with the presence of heterostructures and adsorbed layers on the surface, an unambiguous interpretation of the obtained data is not always possible. To do this, we need both different variants of the EDX analysis, e.g., the analysis of the surface and transverse cleavages, and additional methods, e.g., the analysis of the layer thicknesses, which allow one to more exactly interpret the obtained results. Such additional methods were an optical method of determination of the layer thickness and the X-ray diffraction method.

Figure 1 shows the surface morphology, EDX spectrum, and chemical composition of the SnO_2 film obtained on sapphire in a variant of deposition with the antimony dopant.

It is evident that, in this case, the obtained composition, making allowance for the measurement accuracy, corresponds to the SnO_2 film on Al_2O_3. In contrast with this, the composition of the film obtained on silicon, also in the variant of deposition with the antimony dopant, does not correspond to stoichiometric SnO_2. A substantial excess of oxygen is observed (Fig. 2). A similar pattern is observed for obtaining the TiO_2 films on silicon (Fig. 3). In the last case, the average results over the sample surface are presented along with the standard deviations.



Element	wt %	at %
O K	32.17	61.59
Al K	23.86	27.09
Sn L	41.24	10.64
Sb L	2.73	0.69
Totals	100.00	

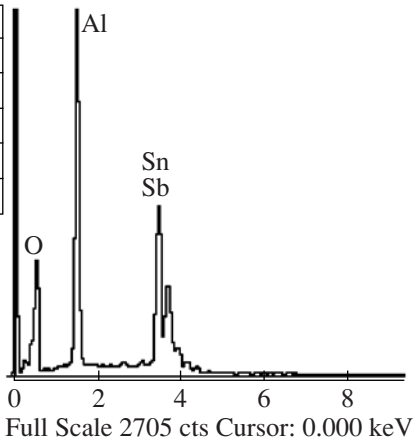
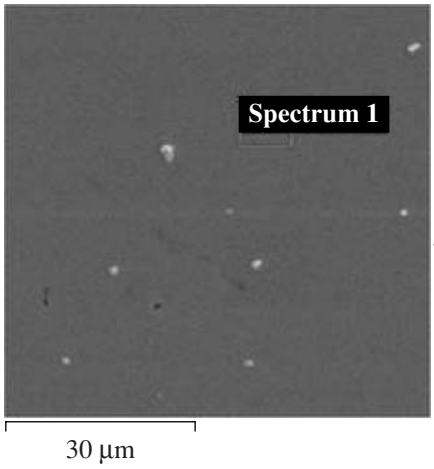


Fig. 1. Surface morphology, EDX spectrum, and chemical composition of the antimony-doped tin oxide film deposited on sapphire.



Element	wt %	at %
O K	31.98	61.52
Si K	24.92	27.31
Sn L	41.46	10.75
Sb L	1.64	0.42
Totals	100.00	

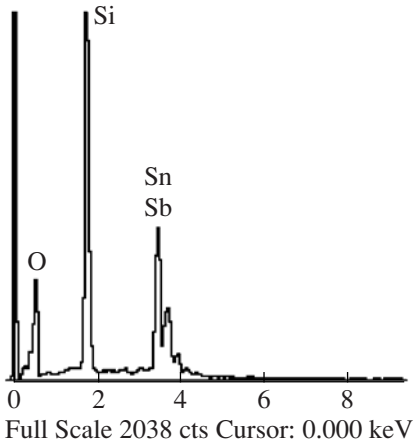
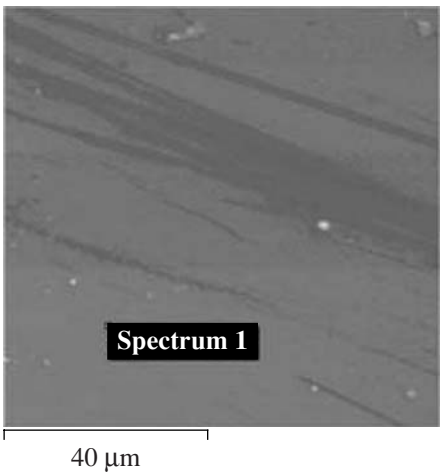


Fig. 2. Surface morphology, EDX spectrum, and chemical composition of the antimony-doped tin oxide film deposited on silicon.



Element	at %
O K	22.6 ± 1.0
Si K	74.7 ± 1.2
Ti K	2.8 ± 0.2

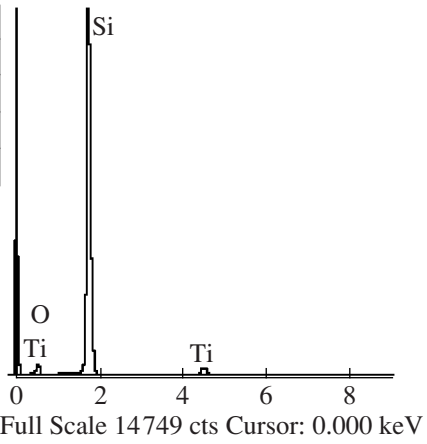


Fig. 3. Surface morphology, EDX spectrum, and chemical composition of the titanium oxide film deposited on silicon.

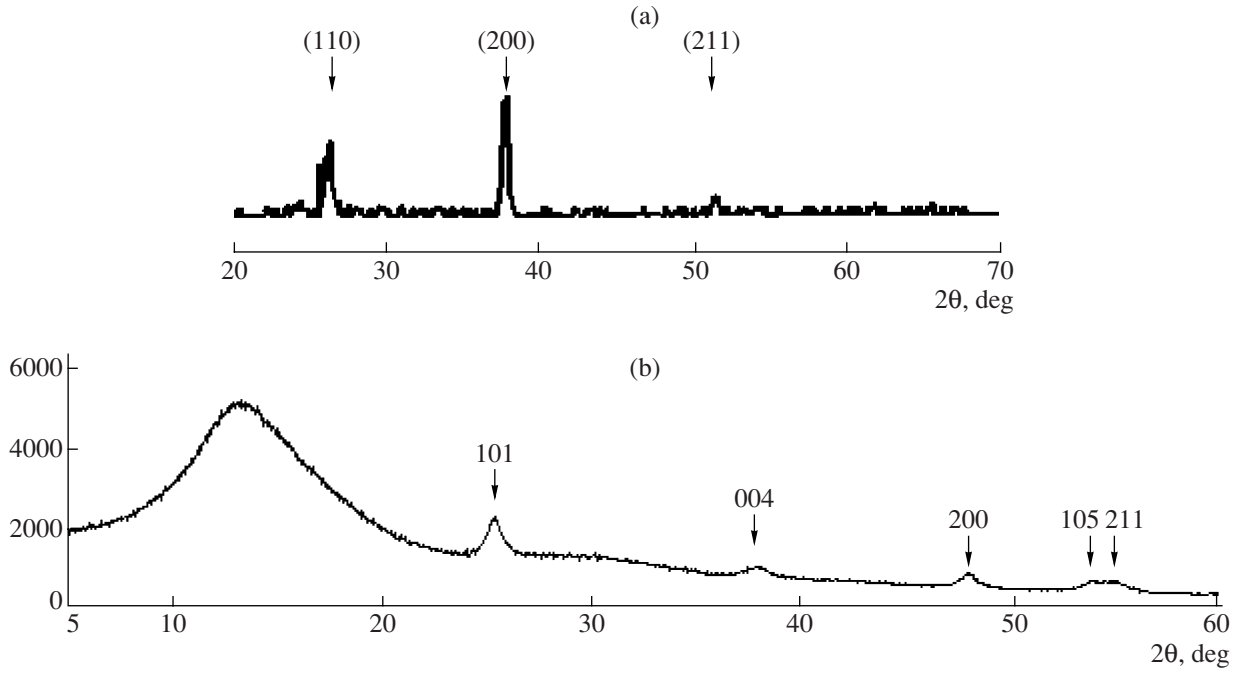


Fig. 4. X-ray diffraction spectra of the films of (a) tin oxide and (b) titanium oxide obtained by pyrolytic pulverization.

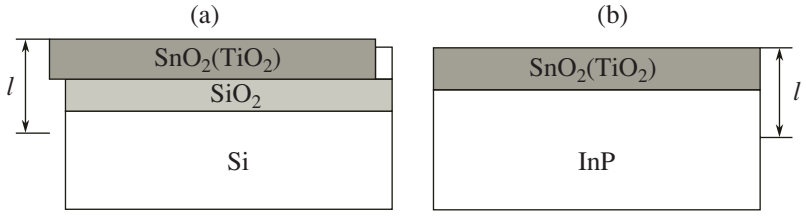


Fig. 5. Schematic image of the oxide–semiconductor structures obtained by pyrolytic pulverization. *l* is the thickness of the layer in which the EDX analysis is performed.

To study the structure, the films of tin and titanium oxides were removed from the surfaces of the substrates and analyzed using X-ray phase analysis, whose results are presented in Fig. 4 and Table 1.

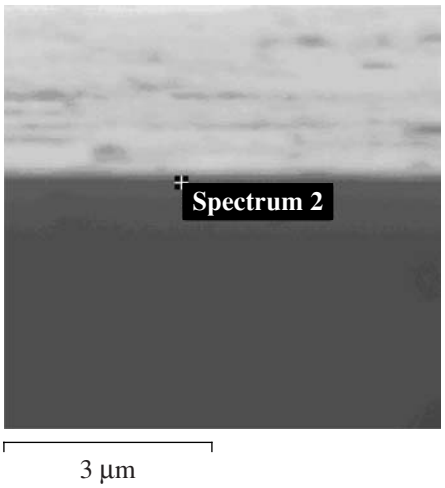
The X-ray diffraction patterns of the surface indicate that the films obtained by pyrolytic pulverization are SnO_2 and TiO_2 oxides and possess the tetragonal crystal structure. The TiO_2 film corresponds to the anatase modification. As for the presence of excess oxygen, it can be associated with the fact that, for deposition on Si, a more complex structure is observed (Fig. 5a), in which the intermediate phase of silicon oxide is observed for deposition of both TiO_2 and SnO_2.

Table 1. X-ray diffraction parameters of titanium oxide films

Peak no.	Miller index, *hkl*	Interplanar spacing, Å
1	101	3.507
2	004	2.371
3	200	1.891
4	105	1.699
5	211	1.667

With the proviso of the correctness of the assumptions made, it seems to be evident that the obtained TiO_2 layer is substantially (by a factor of several times) thinner than the tin oxide layer, which can be judged by the difference in the concentrations (in atomic percent) obtained using this method (compare the data of Figs. 2 and 3).

This can be confirmed by the results of optical measurements given below and the data of the EDX analysis for the films containing the antimony dopant (Fig. 2) and without it (Table 2). According to the results of the



Element	wt %	at %
O K	0.20	0.89
P K	22.33	51.07
Ti K	0.28	0.42
In L	77.19	47.63
Totals	100.00	

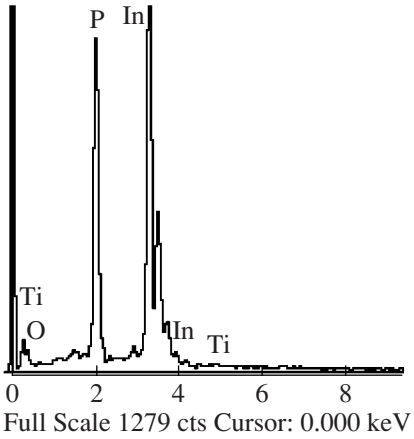


Fig. 6. Microphotograph of the transverse cut, EDX spectrum, and chemical composition of the titanium oxide film deposited on indium phosphide.

optical measurements (the calculation methods will be presented in the following section), the thickness of the SnO_2 films without the antimony additive is 330 nm, and, with the additive, it is 200 nm for the deposition of these films on glass. Exactly the same ratio of the tin concentrations determined by the EDX method takes place for the deposition of the SnO_2 film on silicon (1.64) without antimony and with antimony during the pyrolysis (Fig. 2, Table 2). Under the assumptions made, the thickness of the titanium oxide film with the anatase structure deposited on Si is about 50 nm (see Figs. 2, 4).

The possibility of formation of an intermediate layer of silicon oxide for deposition of the films of titanium oxide on silicon by other methods at the same temperatures that were used in this study was shown more than once. The efficiency of the use of such a structure in photovoltaic systems was also pointed out [8].

In contrast with the deposition on silicon, the intermediate layer does not manifest itself during preparation of TiO_2 films on InP. The results of the elemental analysis of the diagonal cut indicate this fact. The observed stoichiometric ratio between titanium and oxygen equals approximately two (Fig. 6).

Simultaneously, the obtained results can indicate that the film of titanium oxide on InP is even thinner than on silicon because of the lower Ti content (compare the data of Figs. 3 and 6).

Taking into account the qualitative similarity of the processes of formation of the SnO_2 and TiO_2 films, we can suppose that a similar pattern will be also observed for the formation of the SnO_2 films on InP; i.e., the scheme of the forming heterojunction will correspond to that presented in Fig. 5b with the only difference being that the obtained films should be thicker. However, the results of the measurements of the composition of the surface layer after deposition of SnO_2 on InP presented in Fig. 7 contradict the statement on the absence of the intermediate oxide layer, i.e., correspondence to Fig. 5b, since, as follows from the results presented in Fig. 7, excess oxygen is present in this case.

It is evident from the comparison of the data presented in Fig. 7 and Table 2 that, for deposition on InP, the layer of tin oxide is somewhat thinner than for deposition of this oxide on Si but substantially thicker than the titanium oxide layer deposited on InP. As for the presence of excess oxygen and the possibility of formation of the heterostructure with tin oxide and the intermediate oxide layer on InP, which is not observed in the case of deposition of titanium oxide on InP, this question should be answered based on additional investigations.

Optical Properties of Films and Heterojunctions

Transmission spectra were investigated for the obtained SnO_2 and TiO_2 layers. Figure 8 presents such spectra for the SnO_2 layers deposited on glass substrates. The transparency of the undoped layers in this wavelength region reaches 85%, and, for the antimony-doped layers, it falls to 53%. The observed interference

Table 2. Chemical composition of the undoped SnO_2 film deposited on silicon

Element	wt %	at %
O	32.11	71.22
Si	8.80	11.12
Sn	59.09	17.66

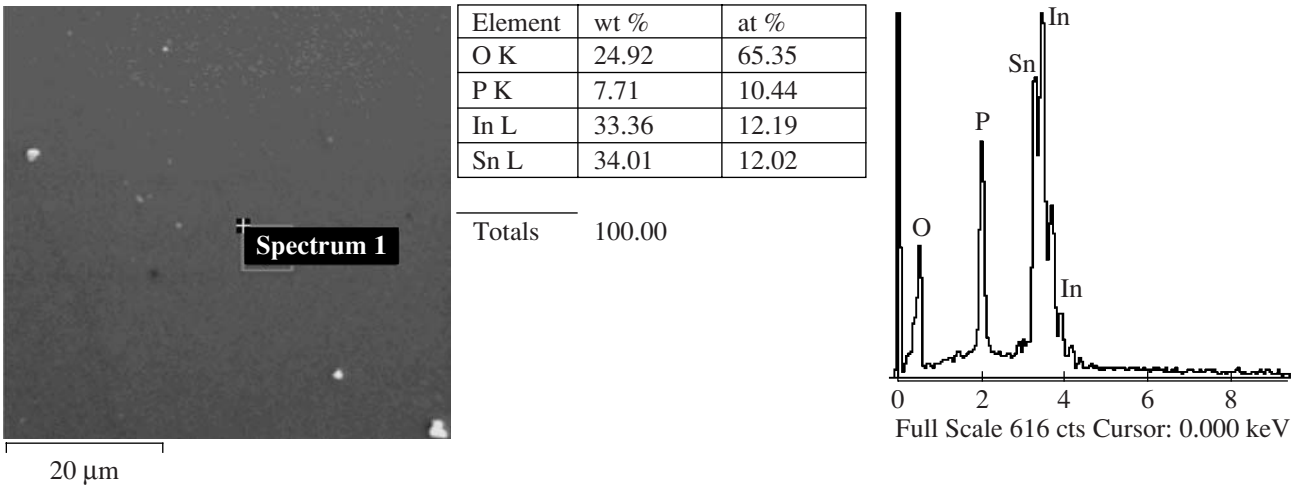


Fig. 7. Surface morphology, EDX spectrum, and chemical composition of the titanium oxide film deposited on indium phosphide.

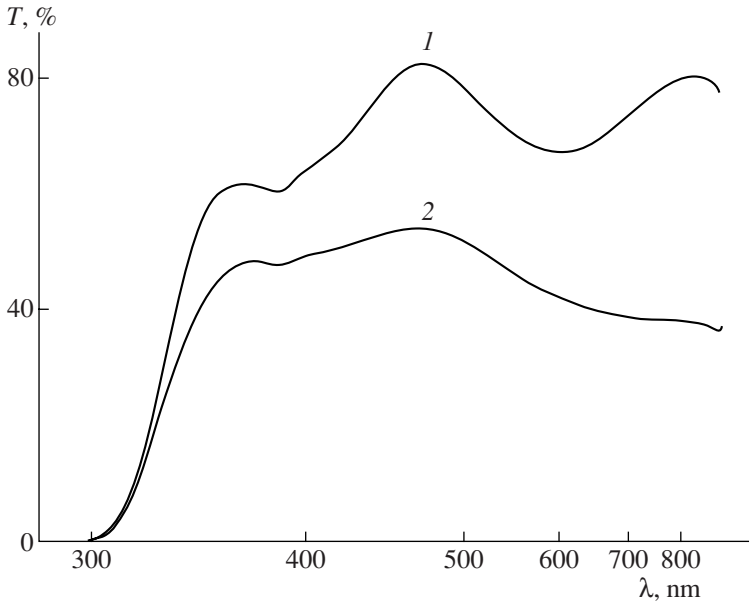


Fig. 8. Transmission spectra of (*1*) the undoped and (*2*) Sb-doped SnO_2 film.

pattern allows one to estimate the thickness D of the SnO_2 films using the known relation [9]

$$D = \lambda_1\lambda_2/(\lambda_1 - \lambda_2)2n, \quad (2)$$

where λ_1 and λ_2 are the wavelengths of the nearest peaks or valleys and n is the refraction index for SnO_2 equal to 2 at a wavelength of 550 nm [10]. The thus obtained thicknesses of the SnO_2 layers are 330 nm for the undoped film and 200 for the doped film.

The corresponding spectra of the films deposited on quartz and sapphire substrates differ by the smoother transparency decay in the region of short wavelengths. The edge of the transmission band at 4.96 eV is independent of the substrate nature in this case. These results allowed us to more exactly determine the band gap of SnO_2 equal to 4.7 eV.

In the case of TiO_2 films deposited on glass and silicon, the spectral distribution of the transmittances and reflectances is presented in Fig. 9. One can see that these films are transparent in the wavelength range of 500–2500 nm. The maximum value of the reflectance equal to 35% is observed at $\lambda = 425$ nm. As the wavelength increases, the reflectance monotonically decreases to 10%.

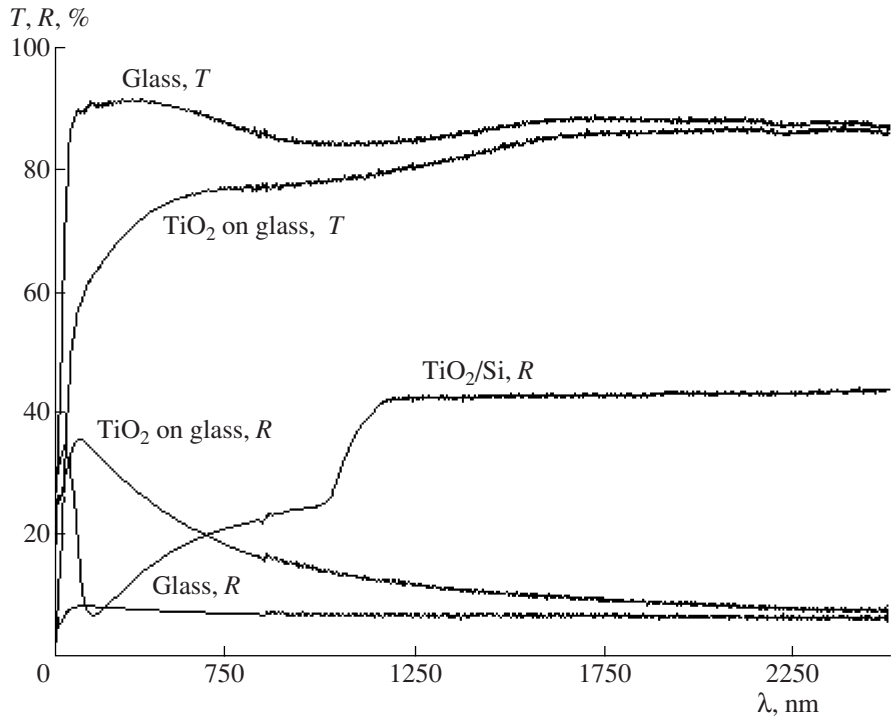


Fig. 9. Spectral distribution of the transmittances T and reflectances R of the titanium oxide films on glass and silicon.

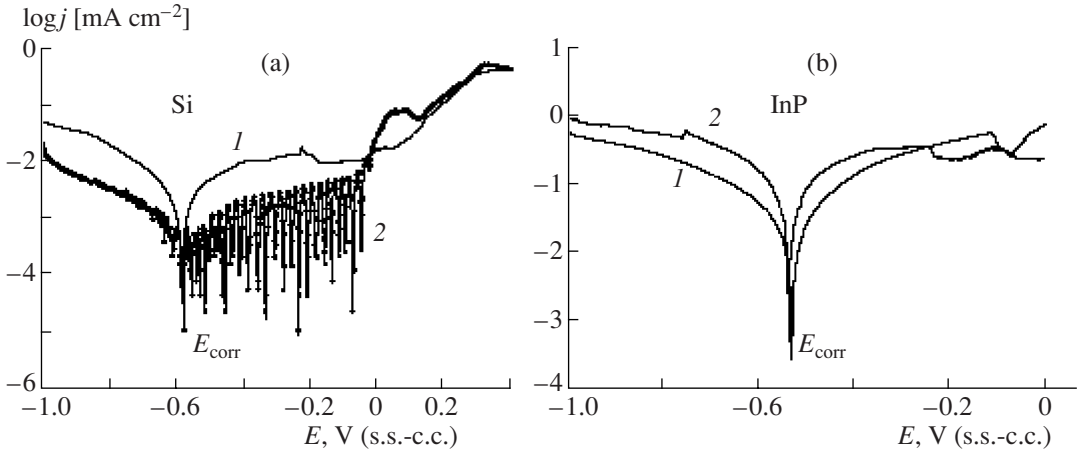


Fig. 10. Corrosion diagrams of (a) silicon ($n_0 = 5 \times 10^{15}$ cm^{-3}) and (b) indium phosphide ($n_0 = 10^{18}$ cm^{-3}) in the chloride–sulfate corrosion solution (*1*) in the dark and (2) in the light.

Corrosion Characteristics

Corrosion tests carried out by the above-described procedures allowed us to judge the efficiency of the obtained heterojunctions from the viewpoint of photocorrosion and photodegradation. Figure 10 shows the voltammetric corrosion diagrams of the narrow-gap semiconductors used as the substrates, and Table 3 gives the characteristics of the corrosion process for the used corrosion medium calculated based on these diagrams.

Table 3 also shows the values of the resistance to the charge transfer obtained based on impedance measurements, which can be considered as a characteristic of the corrosion process for these systems. It is evident

Table 3. Characteristics of the corrosion process in a neutral medium (pH = 6.0) of semiconductor materials and oxide–semiconductor heterojunctions

Material	Voltampermetry					
	E_{corr}, V		j_{corr}, A/cm^2		Resistance to charge transfer, kΩ	
	Dark	Light	Dark	Light	Dark	Light
Si	–0.58	–0.58	2.8×10^{-6}	2.8×10^{-7}	30	164
InP	–0.52	–0.51	3.4×10^{-5}	2.1×10^{-5}	14	7.6
SnO_2/Si	–0.35	–0.43	1.4×10^{-6}	3.1×10^{-7}	260	423
TiO_2/Si	–0.16	–0.03	4.5×10^{-7}	1.6×10^{-6}	300	45
SnO_2/Si	–0.01	–0.02	2.6×10^{-6}	1.7×10^{-5}	74	41

that silicon is much more resistant to photodegradation (photoelectrochemical corrosion) than InP, while their corrosion potentials are close to each other (Fig. 10, Table 3).

The used semiconductor materials had various carrier concentrations (n_0). For example, for Si, it was equal to 5×10^{15} cm^{-3}, and, for InP, 10^{16} and 10^{18} cm^{-3}. In the experiments with high-resistivity samples, oscillations were observed, specifically, those of the anode current in the light (Fig. 10), which can be attributed precisely to a low carrier concentration. It is evident that their periodic generation and recombination are caused by phenomena of passivation and repassivation of the surface under the effect of the light in the anode region of the potentials. At a high carrier concentration (see Fig. 10b), this phenomenon is not observed. It should be noted that the oscillations observed in corrosion experiments with Si in the light are not specific for silicon only. They were also observed in other systems, for example, for InP, if the carrier concentration was sufficiently low.

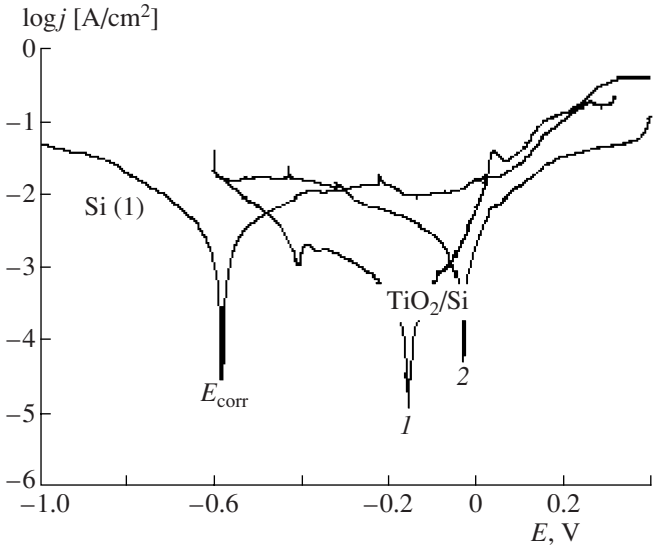


Fig. 11. Corrosion diagrams of silicon and the structure of titanium oxide–silicon (*1*) in the dark and (*2*) in the light.

Deposition of oxides with obtaining the heterojunctions leads to a considerable shift of the corrosion potential into the anode region (Fig. 11, Table 3).

To the largest extent, this is characteristic of the films of titanium oxide on silicon and tin oxide on indium phosphide. The densities of the corrosion currents have the same order of magnitude in this case. The shift of the corrosion potentials into the anode region makes these materials very promising not only from the viewpoint of corrosion but also for electrochemical applications, specifically as photoanodes for photoelectro-chemical obtaining of hydrogen.

The results of the impedance measurements, which were performed only in the light, qualitatively agree with the results of the voltammetric tests, with the data of the chemical analysis, and with the structure of the heterojunctions.

Figures 12–14 show the impedance spectra both for pure materials and for heterojunctions, as well as the corresponding equivalent circuits.

The obtained equivalent circuits demonstrate the formation of various heterojunctions. Specifically, simple systems such as silicon/electrolyte and indium phosphide/electrolyte can be described by a simplest circuit with a single interface (semiconductor–electrolyte) since only one semicircle is observed in the complex plane (Fig. 12). Unlike for InP-based heterojunctions, two semicircles are observed, which corresponds to the equivalent circuit with two barriers (two interfaces, Fig. 13). It seems likely that the assumption made above by the results of chemical analysis with

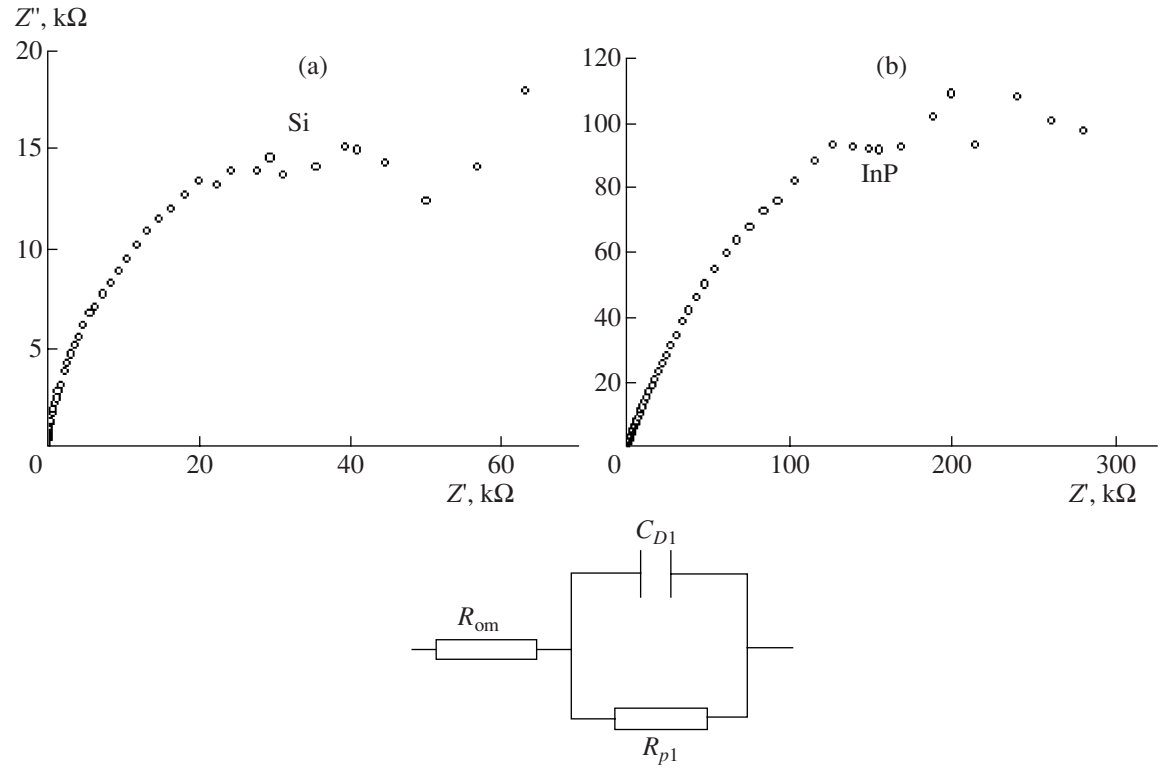


Fig. 12. Impedance spectra of (a) silicon ($n_0 = 5 \times 10^{15}$ cm^{-3}) and (b) indium phosphide ($n_0 = 10^{18}$ cm^{-3}) and the corresponding equivalent circuit obtained in the chloride–sulfate corrosion solution.

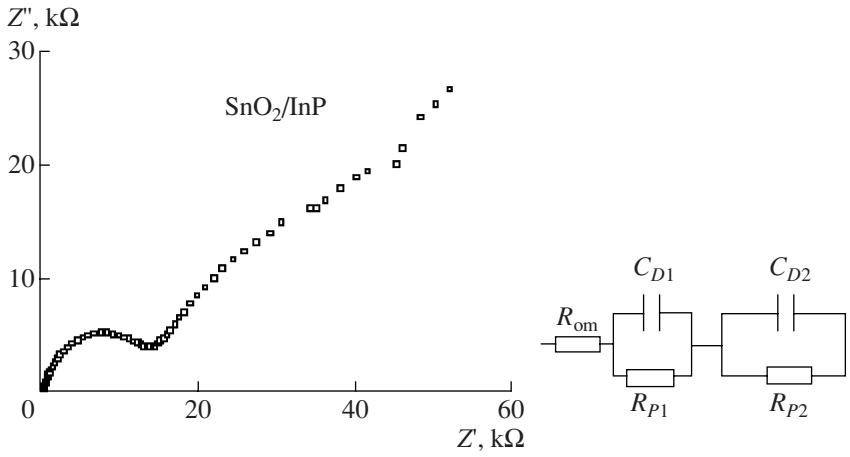


Fig. 13. Impedance spectrum of the SnO_2/InP structure (carrier concentration in InP $n_0 = 5 \times 10^{16}$ cm^{-3}) and the corresponding equivalent circuit.

respect to a relatively simple heterojunction, which is not complicated by the intermediate oxide layer for the systems oxide/InP (see Fig. 5b), is righteous.

For the system SnO_2/silicon, a considerably more complex pattern is observed (Fig. 14). The equivalent circuit involves several junctions and inductance, which corresponds to a more complex heterostructure and the data of the chemical analysis indicating the presence of the silicon oxide layer under the tin oxide layer (see Fig. 5a).

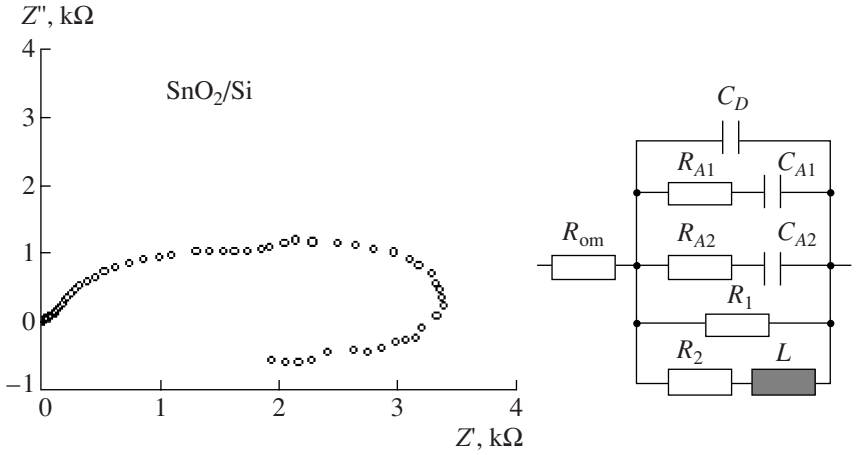


Fig. 14. Impedance spectrum of the SnO_2/Si structure (carrier concentration in Si $n_0 = 5 \times 10^{15}$ cm^{-3}) in the chloride–sulfate corrosion solution and the corresponding equivalent circuit.

CONCLUSIONS

Peculiarities of obtaining the films of tin and titanium oxides, as well as semiconductor structures on their basis, by the method of pyrolytic pulverization are described. The x-ray diffraction data showed that crystalline tetragonal structures are formed in this case (anatase modification for TiO_2). The results of the elemental analysis and impedance investigations of the obtained semiconductor structures in a model chloride–sulfate solution showed that, in the case of oxidation on silicon, the structure oxide/SiO_2/Si is formed and, in the case of deposition on InP, the structure oxide/InP is formed. The results of the corrosion investigations showed that, during the deposition of the above-mentioned oxides on the Si and InP crystals and obtaining the corresponding semiconductor heterostructures, a substantial shift of the corrosion potential into the anode region is observed, which makes them promising materials for photovoltaic applications.

ACKNOWLEDGMENTS

We thank E. Monaiko (National Center of Investigation and Testing of Materials TUM) for help in investigations of the surface of films and structures.

This work was supported by project no. 06.408.02.02P and CRDF-MRDA project no. MOE2-3062-CS-03.

REFERENCES

1. Adeeb, N., Kretsu, I., Sherban, D., Sushkevich, V., and Simashkevich, A., Spray Deposited ITO–CdTe Solar Cells, *Sol. Energy Mater.*, 1987, vol. 15, no. 1, pp. 9–19.
2. Vasu, V., Subrahmanyam, A., Kumar, J., and Pamasamy, P., Spray-Pyrolytic-Grown ITO/InP Junctions: Effects of Tin Doping, *Semicond. Sci. Technol.*, 1993, vol. 8, pp. 437–440.
3. Do Quoc Hung, Bobeico, E., Gorceac, L, Sherban, D., and Simashkevich, A., Solar Cells Based on SIS structures, *Proc. 3rd Int. Workshop on Material Science, Part I*, Hanoi, 1999, pp. 56–59.
4. Gagara, L., Gorcheac, L., Radu, C., Sherban, D., and Simashkevich, A., Photovoltaic Converters of Solar Energy on the Base of SIS Structures, *Proc. Int. Conf. "Euro-Sun 96",* Munchen, 1996, vol. 2, pp. 665–669.
5. Simashkevich, A., Sherban, D., Bruk, L., Bobeico, E., Coval, A., Fedorov, V., and Usatyi Iu, Spray Deposited ITO–*n*-Si Solar Cells with Enlarged Area, *Proc. 20th European PV Solar Energy Conf.,* Barcelona, 2005, pp. 980–982.
6. Grätzel, M., Photoelectrochemical Cells, *Nature*, 2001, vol. 414, pp. 338–344.
7. Badawy, W.A., Improved *n*-Si/oxide Junctions for Environmentally Safe Solar Energy Conversion, *Sol. Energy Mater. Sol. Cells*, 2002, vol. 71, pp. 281–294.
8. Green, M.A., *Silicon Solar Cells: Advanced Principles and Practice*, Sydney: Bridge Printery, 1995.
9. Moss, T., Barrel, G., and Ellis, B., *Semiconductor Optoelectronics*, New York, Halsted Press, 1973.
10. Voronkova, E.M., Grechushnikov, B.N., Distler, G.I., and Petrov, I.P., *Opticheskie materialy dlya infrakrasnoi tekhniki* (Optical Materials for Infrared Technique), Moscow: Nauka, 1965.